DOI: 10.13009/EUCASS2017-332

DOI: ADD DOINUMBER HERE

Basic Analysis of a LOX/Methane Expander Bleed Engine

Marco Leonardi⋆*, Francesco Nasuti*⋆† *and Marcello Onofri*⋆
⋆*Sapienza University of Rome*
Via Eudossiana 18, Rome, Italy
marco.leonardi@uniroma1.it · francesco.nasuti@uniroma1.it · marcello.onofri@uniroma1.it
†Corresponding author

Abstract

As present trends in rocket engine development recommend overall simplicity and reliability as the main design driver, while preserving high performance, expander cycle engines based on the oxygen-methane pair have been considered as a possible upper stage option. A closed expander cycle is considered for Vega Evolution upper stage, while there are no studies published in the literature on methane-based expander bleed cycles. A basic cycle analysis is presented to evaluate the performance of an oxygen/methane expander bleed cycle for an engine of 100 kN thrust class. Results show the feasibility of the system and its peculiarities with respect to the better known expander bleed cycle based on hydrogen.

1. Introduction

The high chamber pressure required to achieve high specific impulse in liquid propellant rocket engines (LRE), has been efficiently obtained by pump-fed systems. Different solutions have been proposed since the beginning of space age and just a few of them has found its own field of application. In these systems the pumps are driven by gas turbines whose power comes from two possible sources: combustion or cooling system. The different needs for the specific applications (booster, sustainer or upper stage of different classes of rockets) led to classify pump-fed LRE systems in open and closed cycles, which differ because of turbine discharge pressure.[14,16] Closed cycles are those providing the best performance because the whole propellant mass flow rate is exploited in the main chamber. This can be achieved at the cost of a more complicated architecture than open cycles and of a quite higher maximum system pressure. Conversely, open cycles are simpler because they decouple the flow path in two branches: the main one, with most of propellant, to be used in the main chamber; and the secondary one whose only goal is to provide power to turbines. The cost for open cycles is that part of the propellants is not exploited in the main chamber with a consequent performance penalty.

Considering the possible power sources for turbines, architectures relying on heat extracted from cooling system are particularly interesting when looking for simple and restartable engines, as they do not need combustion devices other than the main chamber. Pump-fed engines with turbine power extracted from the cooling system are referred to as expander cycles and have been developed for upper-stage use, because of their limitations in terms of available power when compared with their gas-generator or staged combustion cycle counterparts. Expander cycles (EC) are thus simple and reliable engine cycles characterized by the absence of any additional combustion devices. The absence of combustion gases allows for easier start-up sequences, and avoids the need of controlling the mixture ratio of the gas generator. Moreover, while in a turbine driven by combustion products the presence of water vapor could cause the turbine to freeze between restarts, this is not the case for expander cycles. Therefore, purge operations are not necessary, and maintenance costs decrease consequently. However, expander cycles are not the best solution for high thrust levels, due to the limitations related to the power that can be extracted from cooling process of the combustion chamber. In fact, the energy available to drive the turbopumps is limited by the thrust chamber heat transfer. A further important consideration is that only a limited number of rocket fuels are able to extract power from the cooling system and get a significant chamber pressure increase. They are the lightest liquid fuels as hydrogen, methane and propane.[16,22]

For the mentioned reasons expander cycles have been adopted for upper stage rocket engines like those of RL10 family,[20] the Vinci engine[2,19] and those of the LE5 family.[7,10–13,15,21] While RL-10 and Vinci rely on a closed cycle architecture, LE5-A, LE5-B is the only production engine family which is based on “open expander” (or “expander bleed”) cycle. In all these cases the propellant combination is hydrogen/oxygen and therefore these expander systems rely on the best available coolant that is hydrogen. More specifically, RL-10 family and Vinci engines aim at the best

DOI: 10.13009/EUCASS2017-332

performance with their closed architecture, whereas LE5-B aims to a good performance and maximum simplicity with its open architecture.

Focusing on the search for simple and reliable upper stage engines, the choice could be oriented towards expander bleed systems. However, from the point of view of ease of handling and cost, hydrogen fuelled systems could not be the best choice. To conjugate the advantages of expander systems together with better performance than storable propellant engines, green propulsion, and low cost, the optimum choice would be to rely on methane engine. Except hydrogen, methane is in fact the best propellant for use in expander cycle systems. Today there is much interest in this fuel for different applications, from boosters −to combine relatively high density together with high performance and suitability to reuse−, to space exploration −because of the theoretical possibility of in-situ methane production on Mars−, and finally to upper stage, especially because of its higher density, higher boiling point and reduced handling and safety constraints compared to hydrogen,[5] despite its lower performance.

Although no launcher upper stage based on methane fuel has yet flown, the idea of realizing such an engine is around since many years.[4,17] Ground testing of such systems is being carried out, as for example is the case of the upper stage LM10-MIRA[18] foreseen for the evolution of VEGA launcher (VEGA-E). In all the above mentioned studies and testing, attention was devoted to maximum performance and therefore all refer to the closed version of the expander cycle. On the other hand, to the Authors knowledge, no studies have been published on expander bleed systems based on methane.

Aim of the present study, is to carry out a basic analysis of the expected performance and limits of an oxygen/methane expander bleed systems. Attention is focused on the VEGA-E upper stage class engine, that is the goal is to evaluate the performance loss and the possible advantages of an expander bleed system as compared to the reference LM10-MIRA upper stage. Performance analysis at steady-state is carried out with simplified approaches for most of the system components. A deeper attention is devoted to the cooling system that is a critical component to evaluate performance of all the expander cycle systems.

2. Engine configuration

Goal of the present analysis is to evaluate the performance of an expander bleed engine satisfying a similar set of requirements as the LM10-MIRA engine.[18] It is certainly expected that the system will provide a lower specific impulse with a consequent theoretical cost in terms of final payload, but a simpler system should be obtained. The set of requirements assumed for the present study are taken from the literature and summarized in Table 1 and include the thrust level F, the minimum mixture ratio (O/F), and the maximum allowed wall temperature T_w. Dimensional

Table 1: Engine basic requirements

Thrust, F [kN]	100
Overall mixture ratio, (O/F)	≥ 3.4
Wall temperature, T_w [K]	≤ 800
Engine length, L [m]	≤ 1.9
Engine maximum diameter, D_e [m]	≤ 1.3

constraints are rather tight to get a high performance with an expander bleed cycle, because they hide a strong constraint in term of maximum admissible nozzle expansion ratio. For this reason the equality sign will be considered for engine length L and maximum diameter D_e, to exploit the maximum nozzle area ratio. To analyze the system a number of assumptions must also be made about the overall architecture. For the present study, taking advantage from the higher density of liquid methane compared to liquid hydrogen, a system with a single turbine moving both fuel and oxidizer pumps is considered, according to the schematic of Fig. 1. For an effective cooling of the thrust chamber the whole fuel mass flow rate flows in the cooling system. Then a second part of cooling is achieved by a fraction of the coolant mass that is brought at higher temperature before moving the turbine (see also Fig. 2). The schematic follows therefore the expander bleed cycle scheme referred to as “nozzle expander bleed”.[8]

3. Basic analysis

In a basic analysis pressure losses and turbomachine efficiencies are assumed as known from experience. To account for pressure losses ahead of thrust chamber two parameters a_f, a_o are introduced that will be referred to as pump head coefficient for the fuel and oxidizer pump, respectively. These coefficients allow one to express the pump head as proportional to chamber pressure. In fact, the pressure rise across the pumps has to include pressure drop through lines

DOI: 10.13009/EUCASS2017-332

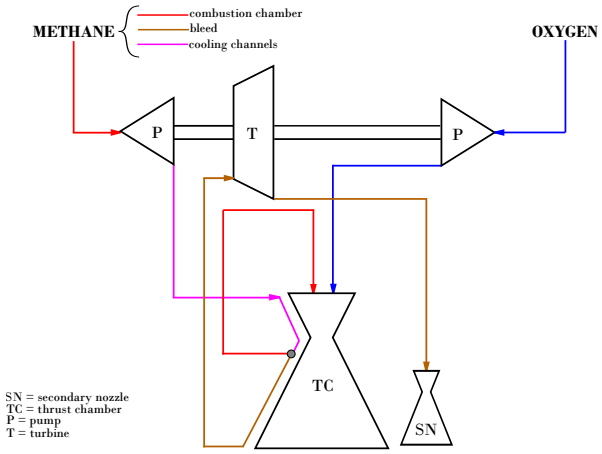

Figure 1: Schematic of the basic nozzle expander bleed system with a single turbine.

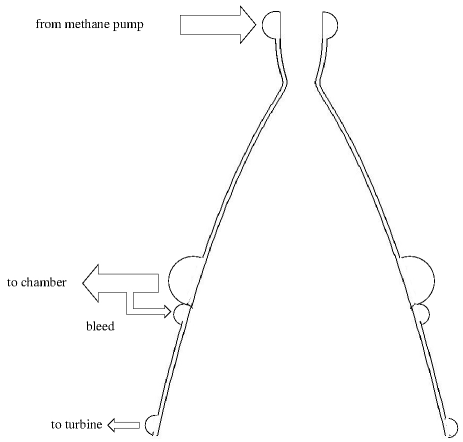

Figure 2: Schematic of the basic nozzle expander bleed cooling system.

(Δp_{line}), cooling system (Δp_{cool}) and injectors (Δp_{inj}). So the pump head can be expressed as the difference between the chamber pressure (p_c), increased by the above mentioned pressure drop and the tank pressure (p_{tank}). It can be written for the fuel and oxidizer pump (subscript f and o, respectively) as:

- Methane pump

$$\Delta p_f = p_c + \Delta p_{f,inj} + \Delta p_{f,line} + \Delta p_{f,cool} - p_{f,tank} \approx a_f p_c \tag{1}$$

- Oxygen pump

$$\Delta p_o = p_c + \Delta p_{o,inj} + \Delta p_{o,line} - p_{o,tank} \approx a_o p_c \tag{2}$$

where cooling system pressure drop only appears for fuel, which is therefore expected to experience a higher pressure loss between the pump exit and the combustion chamber. Note that Δp_{line} and p_{tank} are usually terms quite smaller that the others in Eqs. (1) and (2) and therefore can be neglected in a first approximation, while Δp_{cool} and Δp_{inj} can typically be considered as proportional to p_c.

With these assumptions and with the assumption made of constant a_f and a_o, the balance between turbine generated power and the pump power provides a simple relation among the remaining unknown parameters. They are the turbine inlet temperature T_t, the turbine expansion ratio $\tau^{\gamma/(\gamma-1)}$, the amount of fuel mass flow directed to turbine $\dot{m}_t$ and the chamber pressure p_c. More specifically the power balance can be written as:

$$\dot{m}_f \frac{\Delta p_f}{\rho_f \eta_{p,f}} + \dot{m}_o \frac{\Delta p_o}{\rho_o \eta_{p,o}} = \dot{m}_t \eta_t c_{p,t} T_t (1 - \tau) \tag{3}$$

that, using Eq. (1) and Eq. (2), and introducing the overall oxidizer to fuel mass flow ratio $O/F = \dot{m}_o/\dot{m}_f$, and the mass fraction diverted to turbine $x = \dot{m}_t/(\dot{m}_o + \dot{m}_f)$, can be rearranged as:

$$\left[\frac{a_f}{\rho_f \eta_{p,f}} + (O/F) \frac{a_o}{\rho_o \eta_{p,o}} \right] p_c = x[1 + (O/F)] \eta_t c_{p,t} T_t (1 - \tau) \tag{4}$$

that clearly relates chamber pressure to the power generated by the turbine, which is proportional to turbine mass flow rate, expansion ratio, inlet temperature, and efficiency η_t. Note that turbine power also depends on the turbine gas specific heat $c_{p,t}$. It is evident from Eq. (4) that once constant values are assumed as a first approximation for a_f, a_o, η_t, $\eta_{p,f}$, $\eta_{p,o}$ and $c_{p,t}$, for any overall O/F and x there will be a benefit in terms of chamber pressure by considering the maximum allowed T_t and the maximum turbine expansion ratio (minimum τ)[1].

[1]Note that the ideal total temperature ratio τ is defined on the basis of isentropic total-to-static efficiency. In this case the relationship between total temperature ratio and static-to-total pressure ratio is obtained assuming isentropic expansion:

$$\tau = \frac{T_{t,exit}}{T_t} = \left(\frac{p_{t,exit}}{p_{t,0}} \right)^{\left(\frac{\gamma-1}{\gamma}\right)} \tag{5}$$

In this expression the subscript $()_{exit}$ refers to turbine exit conditions, whereas inlet conditions are reported for the sake of shortness without subscript. Note that subscript $()_0$ is also shown for pressure to emphasize that the total value is considered at the inlet whereas the static value is considered at the exit. Only total temperatures are considered so no subscript is used to emphasize the total temperature values.

DOI: 10.13009/EUCASS2017-332

The overall specific impulse provided by the engine, I_{sp}, is a weighted average value between main and secondary jet, as in all open cycles:

$$I_{sp} = \frac{F}{g_0 \dot{m}_p} = \frac{F_1}{g_0 \dot{m}_p} + \frac{F_2}{g_0 \dot{m}_p} = \frac{(\dot{m}_p - \dot{m}_t) I_{sp,1}}{\dot{m}_p} + \frac{\dot{m}_t I_{sp,2}}{\dot{m}_p} = I_{sp,1} - x(I_{sp,1} - I_{sp,2}) \tag{6}$$

where g_0 is the standard gravity, $\dot{m}_p$ is the overall propellant mass flow rate, $I_{sp,1}$ is the specific impulse of the main chamber and $I_{sp,2}$ the specific impulse provided by the exhaust of the secondary jet. For the best vacuum operation performance in principle the goal would be maximizing chamber pressure, that means maximizing the expansion ratio for the constraints given in Table 1, which finally results in an increase of thrust coefficient and thus of specific impulse. However, taking into account of Eq. (6), for an open cycle this goal is no longer obvious: a compromise must be found because of the secondary jet mass flow rate that is not exploited in the main chamber. In fact, the lower temperature and the limits in the possible expansion ratio of secondary jet leads to a quite lower specific impulse of the secondary jet, if compared to that of the main and the higher the pressure the higher is the expected secondary jet contribution to specific impulse (because of the higher secondary mass flow rate) in Eq. (6). Here, the main chamber specific impulse is obtained by CEA software,[9] with chamber pressure and of $(O/F)_1$ as input, whereas the nozzle supersonic area ratio is selected as a function of the chamber pressure itself, to satisfy geometry and thrust constraints. By introducing the main chamber thrust coefficient $c_{F,1} = F_1/(p_c A_t)$, with A_t the nozzle throat cross section area and F_1 the contribution to thrust of the main chamber, the area ratio is $\varepsilon = A_e/A_t$ is changed iteratively up to reach a value satisfying the constraint of Table 1 in terms of maximum exit area $A_e = \pi D_e^2/4$ and thrust $F = F_1 + F_2$. Simple algebra allows in fact to express:

$$A_e = \frac{\varepsilon F}{p_c c_{F,1}} \left[1 + \frac{x}{1-x} \frac{I_{sp,2}}{I_{sp,1}} \right]^{-1} \tag{7}$$

The value of A_e is evaluated from this expression for each tentative value of ε, because given $(O/F)_1$, p_c and ε, CEA provides the corresponding values of $c_{F,1}$ and $I_{sp,1}$, while $I_{sp,2}$ is separately evaluated by the turbine exit conditions (function of T_t and τ) and the assumed fixed secondary nozzle area ratio. When the converged value of ε is found also the corresponding value of $I_{sp,1}$ is obtained and the engine specific impulse can be computed by Eq. (6). Note that the computation of performance by CEA software is obtained assuming equilibrium conditions in the combustion chamber and up to nozzle throat and frozen flow in the divergent section.

In this framework, it is worth underlining the importance of having high temperatures at turbine inlet: chamber pressure is linearly increasing with T_t, and consequently the performance of the main chamber; the secondary jet performance increases with T_t as well, for a given τ, because of the higher total temperature in the secondary nozzle.

It is also worth noticing that the constraints of Table 1 influence the possible range of the turbine to main mass flow ratio, x. In fact, moving the main chamber mass flow ratio $(O/F)_1$ toward values far from the optimum value would lead to a reduction of performance, despite the pressure increase. The relation between main oxidizer to fuel mass flow rate ratio $(O/F)_1$, overall oxidizer to mass flow rate ratio (O/F) and the ratio x is the following:

$$(O/F)_1 = (O/F) \left\{ \frac{1}{1 - x[1 + (O/F)]} \right\} \tag{8}$$

as can be easily shown.

To identify a reasonable operating point, suitable values of efficiencies, pressure loss, fluid properties and turbine expansion ratio are chosen according to Table 2, whereas x is changed parametrically and p_c and I_{sp} are obtained as results of the analysis. Values of liquid densities as well as the constant pressure specific heat of methane at the expected

Table 2: Expander bleed system specifications

	Fuel	**Oxidizer**
ρ [kg/m^3]	418.5	1143.0
a	1.6	1.3
η_p	0.7	0.7
η_t	0.6	
$c_{p,t}$ [J/kg K]	3336	
τ	0.64	
T_t [K]	600	
(O/F)	3.4	

DOI: 10.13009/EUCASS2017-332

turbine inlet temperature of 600 K are taken from NIST database.[1] The temperature of 600 K has been assumed as the highest that could ensure that the maximum wall temperature is kept below 800 K, as per engine requirements Table 1.[18] The value of turbine temperature ratio is such that supersonic flow is obtained at the exit of secondary jet at sea level conditions, that also guarantees the absence of condensation of the secondary jet. This assumption has been selected after a separated parametric analysis, that is not reported here for the sake of brevity, and because attention is focused here to the evaluation of basic performance. A final optimization of the cycle would instead require a deeper analysis of the behavior and design of all the components of the system. As mentioned, methane losses are greater than the oxygen ones because of the pressure losses in the cooling channels, thus the value of methane pump head coefficient a_f is assumed as greater than oxygen pump head coefficient a_o.

The remaining quantities linked to each other by Eq. (4) and Eq. (8) are $(O/F)_1$, (O/F), x and p_c. Here it can be observed that the best performance of the main chamber is obtained at $(O/F)_1$ lower than the minimum allowed $(O/F) = 3.4$. For instance, if one assume, as done in this study, shifting equilibrium up to throat and frozen flow in the divergent section, it can be shown that $I_{sp,1}$ is maximum at $(O/F)_1 \sim 2.85$ for the expected range of pressure and area ratio. Therefore, it is impossible that the best overall performance is obtained with $(O/F) > 3.4$. In fact, because of the secondary flow the resulting $(O/F)_1$ will be higher than the prescribed value of 3.4, and thus it can be inferred that the best operating conditions will be those obtained assuming the equality sign in Table 2 also for the parameter (O/F). It is assumed therefore $(O/F) = 3.4$.

At this point a parametric analysis is made changing the values of x to obtain the corresponding values of p_c, I_{sp}, $(O/F)_1$ and all the other properties of the system. The results of parametric analysis are shown in Fig. 3. As shown from Eq. (4), p_c is linear with x, so that an increase of x would yield an increase of main chamber $I_{sp,1}$. However, keeping (O/F) constant also yields a change of $(O/F)_1$, which increases for increasing x. Being for a given p_c the maximum $I_{sp,1}$ for $(O/F)_1 \sim 2.85$, because of this change of $(O/F)_1$, an increase of x would yield a decrease of $I_{sp,1}$. Moreover, the weight of secondary flow performance penalty increases for increasing x also contributing to a reduction of the overall I_{sp} for increasing x. Because of these contradictory effects of the amount of mass flow rate used to drive the turbine, a condition with maximum I_{sp} is shown in Fig. 3. More specifically, an optimum condition −assumed as

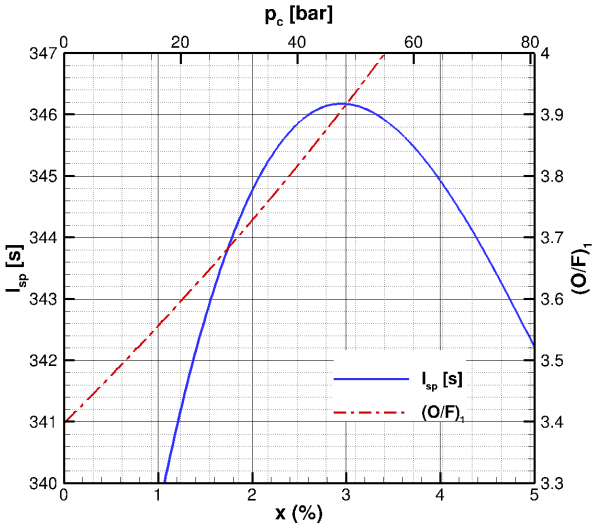

Figure 3: Specific impulse and main chamber mixture ratio as a function of x (p_c)

the reference working point− is obtained at $x = 2.96\%$, $(O/F)_1 = 3.9$, $p_c = 48$ bar, resulting in $I_{sp} = 346$ s, that is about 20 s less than the expected closed cycle specific impulse (see also Table 3).

4. Cooling system analysis

Once the reference working point is defined, an analysis is carried out on the cooling system to verify the assumptions made. In particular, aim of the following analysis is to understand if the temperature T_t can be reached by safely cooling the thrust chamber walls and what is the expected level of pressure loss in the cooling system. These quantities are all strongly dependent on the cooling system design, therefore many possible solutions may satisfy the overall requirements, though featuring different properties that make some of them to be preferred. The capabilities of the

DOI: 10.13009/EUCASS2017-332

Table 3: Reference working point results

x	2.96%	p_c [bar]	48
D_t [m]	0.116	I_{sp} [s]	346.2
$\dot{m}_o$ [kg/s]	22.72	$\dot{m}_f$ [kg/s]	6.69
$\dot{m}_1$ [kg/s]	5.82	$\dot{m}_2$ [kg/s]	0.87
ε_1	125	ε_2	20
$I_{sp,1}$ [s]	352.5	$I_{sp,2}$ [s]	141.4
$(O/F)_1$	3.9	$(O/F)_2$	0.0
F_1 [kN]	98.8	F_2 [kN]	1.2

cooling systems in terms of coolant temperature increase, pressure loss and maximum wall temperature are evaluated using the thrust chamber and cooling system components of the software EcosimPro.[6] The geometry of the nozzle diverging sections is assumed as that of a truncated ideal contour nozzle (see Fig. 2), suitably designed using the method of characteristics on the basis of the results obtained in the foregoing section for the throat diameter D_t and nozzle area ratio, ε_1. The whole nozzle profile design considers a 0.5 m allowance for the combustion chamber and converging nozzle sections, such that the nozzle divergent length is 1.4 m.

To make a parametric analysis on the possible cooling system choice, some assumption has to be made about the channel cross section shape and its possible variation along channel length. Moreover, some constraint have to be enforced, as for instance, minimum/maximum width of channel walls, minimum/maximum channel width and height, minimum/maximum channel aspect ratio (channel height to width ratio), depending on overall engine weight, structural constraints, overall engine size.

For the present analysis the coflow configuration shown in Fig. 2. is considered. The first part (main cooling system) mainly devoted to cooling, with high mass flow rate, and a second part (nozzle extension cooling) where a small amount of fuel is further heated before going towards turbine. The coolant mass flow rates will be based on the overall fuel mass flow rate $\dot{m}_f$ and on the bleed mass flow rate $\dot{m}_t$ reported in Table 3.

4.1 Main cooling system

Channel geometry is changed parametrically with the constraints reported in Table 4. In the parametric analysis the

Table 4: Cooling channel analysis data

Fin thickness at throat section, t_t [mm]	≥ 1.0
Channel base width at throat section, b_t [mm]	≥ 1.0
Number of cooling channels, N	≤ 184
Channel Aspect ratio at throat, AR_t	4
Mass flow rate of chamber cooling, $\dot{m}_{f,cool}$ [kg/s]	3.35-6.69
Axial distance of the main cooling channel exit from throat, x_{cool} [m]	0.4
Liner wall material	copper alloy
Closeout wall material	inconel

fin thickness t_t is assumed constant and equal to its minimum value, whereas the number of cooling channels N is varied from 135 to 184 with the consequent change of channel base width b_t (see Fig. 4 for the definition of geometric parameters). The channel height at throat is obtained subsequently, because the channel aspect ratio at throat $AR_t = h_t/b_t$ is assumed constant in the parametric analysis. Note that the channel height and fin thickness are assumed as constant along the channel for each considered value of N. The overall mass flow rate flowing in channels is also changed as a second variable parameter in the analysis. In this case, part of the coolant bypasses the cooling system and goes directly to the combustion chamber. Finally, for heat input from hot gas side, Bartz equation[3] is assumed and evaluated from CEA software solution for the 1D flow evolution (shifting equilibrium from injection to throat and frozen composition from throat to exit).

The results of the analysis show the expected decreasing trend of the wall temperature with increasing number of channels and coolant mass flow rate (Fig. 5). In fact, it can be easily shown that overall cross section area decreases for increasing N and as a consequence flow velocity in the channels increases improving cooling and increasing at the same

DOI: 10.13009/EUCASS2017-332

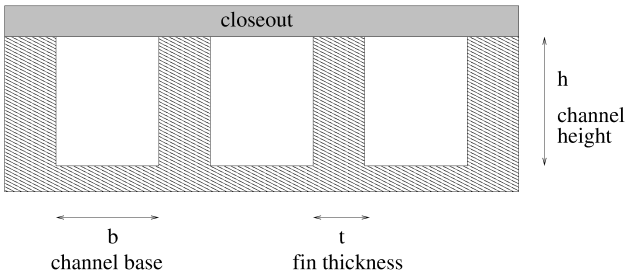

Figure 4: Quantities defining channel cross section

time the pressure loss. Similarly, velocity, and as a consequence heat exchange, increase for increasing coolant mass flow rate for a given cross section area. The improved heat exchange also causes an increase of coolant temperature at the main cooling system exit (T_{out}). This increase is rather small (about 20 K) for changing N, whereas it is much more evident for changing coolant mass flow rate. Pressure drop has an opposite trend if compared to wall temperature. Nevertheless, the pressure drop through the channel is always resulting less than 7 bar. As can be noticed the cooling

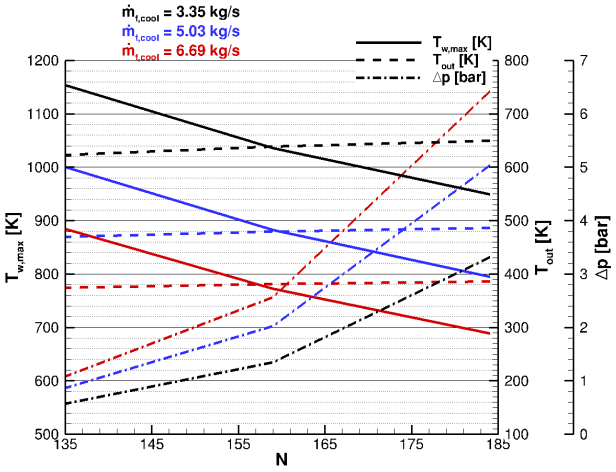

Figure 5: Parametric analysis for varying $\dot{m}_{f,cool}$, and N

conditions are very satisfactory as the maximum wall temperature can be made safely lower than the allowed maximum value.

The best configuration is that showing the maximum number of channels and maximum coolant mass flow rate as this guarantees the minimum value of the maximum wall temperature, although with maximum pressure drop. However, also in this case, the pressure drop is relatively small, well within the margin foreseen in the coefficient a_f in the foregoing section.

Starting from this "best" configuration of the main cooling system (i.e. $N = 184$), a second analysis is carried out to evaluate the role of channel area ratio on the overall performance for the cases of $\dot{m}_{f,cool} = 5.03$ and $\dot{m}_{f,cool} = 6.69$. All data included in the analysis are those of the previous one, except the channel aspect ratio, which is changed parametrically between 2.5 and 4.5, thus resulting in a variation of channel height. The results of the analysis show that despite the change of channel cross section with AR_t the fuel temperature at channel exit remains practically unchanged. On the other hand, reducing AR_t, and thus the channel cross section, yields a slight decrease of maximum wall temperature, with a much more pronounced increase of pressure loss. Pressure loss remains under a 10 bar threshold for $AR_t \gtrsim 3.4$ in case of $\dot{m}_{f,cool} = 6.69$ and for $AR_t \gtrsim 3.0$ in case of $\dot{m}_{f,cool} = 5.03$. Accepting 10 bar pressure drop with lower AR allows to decrease of about $20 - 30$ K the maximum wall temperature, which is now about 650 K for the case without coolant bypass in the main cooling system and 790 K for the case where 1.66 kg/s of fuel bypass the cooling system ($\dot{m}_{f,cool} = 5.03$).

DOI: 10.13009/EUCASS2017-332

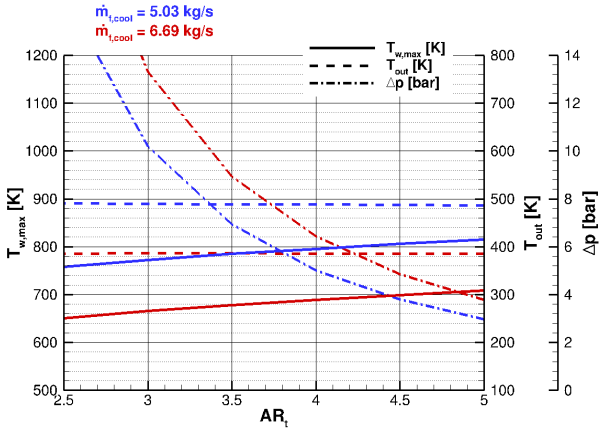

Figure 6: Parametric analysis for varying AR_t, with $N = 184$

4.2 Nozzle extension cooling

To keep the thrust chamber in a safe range of wall temperature (below 800 K), the exit flow temperature from the main cooling system is still too low compared to that assumed in the basic system analysis. In fact, the assumed turbine inlet temperature in the foregoing section is $T_t = 600$ K, compared to the methane temperature at the exit of the main cooling which is less than 400 K for the case without bypass, which provides the lowest wall temperature. Increasing of the enthalpy of the bleed fuel used to drive turbine, is achieved by the cooling of nozzle extension. Due to the lower thermal load in this part of the nozzle, it is convenient to consider a different material, which is able to withstand safely higher temperatures, and thus allows the coolant to reach higher temperatures, and also allows for a lower weight than copper alloys. Inconel is selected in this study, whose properties are taken from the literature. For the nozzle extension cooling, a channel with axial length of 1 m (from the axial position where the main cooling ends, at $x = 4$ m, up to the nozzle exit, at $x = 1.4$ m) is considered. Because of the larger and increasing diameter, the fin thickness is assumed as constant along the channel; the value of $t = 2$ mm is considered for each case of the parametric analysis. In the

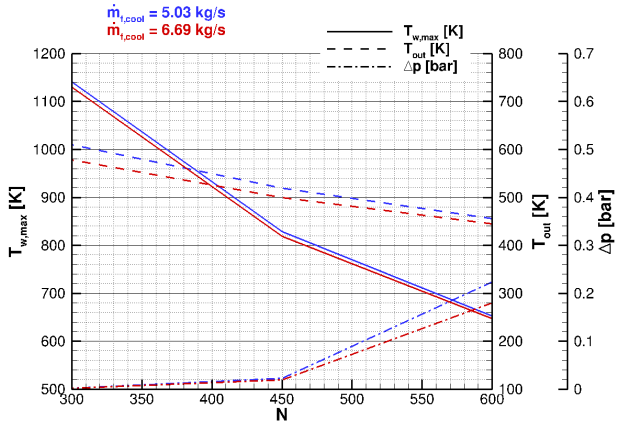

Figure 7: Temperature and pressure behavior for changing number of channels in the nozzle extension cooling as resulting from two configurations of main cooling system: $\dot{m}_{f,cool} = 6.67$ kg/s with $AR_4 = 3.4$ and $N = 184$; $\dot{m}_{f,cool} = 5.03$ kg/s with $AR_4 = 3.0$ and $N = 184$.

parametric analysis the number of channels N is left to vary here between 300 and 600. The channel cross section is assumed as squared ($AR = 1$ or $b = h$, all along the channel), such that also the channel height and cross section area increases when moving towards the nozzle exit.

The results of the analysis are shown in Fig. 7. Note that for both coolant mass flow rates the AR_t leading to

DOI: 10.13009/EUCASS2017-332

10 bar pressure loss has been selected in for the main cooling system together with the maximum number of channels $N = 184$. For the nozzle extension cooling the best solution is that of keeping the number of channels as small as possible. This is because a smaller number of channels yields a higher cross section area and in turn lower flow velocity and poorer cooling. In fact, the goal is here more focused towards coolant heating rather than to the wall cooling. In fact, if one consider the case with the whole fuel flowing in the main cooling system ($\dot{m}_{f,cool} = 6.67$ kg/s), the solution with $N = 300$ in the nozzle extension cooling leads to negligible pressure drop together with an exit temperature $T_t = 580$ K, and a maximum wall temperature of 1130 K. To reach the temperature of 600 K, a possible solution is to get higher temperature at the main cooling system exit. It has been shown before that if one assume that some of the fuel bypasses the cooling system, for instance assuming $\dot{m}_{f,cool} = 5.03$ kg/s, the temperature of the coolant an the main cooling system exit is about 100 K higher, reaching the value of 490 K. This main cooling system with bypass still satisfies the requirement of maximum wall temperature, being the corresponding value close to the upper limit of 800 K (see Fig. 5). Exploiting this higher inlet temperature for the nozzle extension cooling, a higher exit coolant temperature becomes easier to achieve. Looking at Fig. 7, it can be easily seen that the exit temperature of about 600 K can be obtained with $N = 315$, and with a resulting maximum temperature which is reduced to 1110 K. It is worth underlining that the flow is quite slow in the nozzle extension cooling and as a consequence pressure loss is negligible (the maximum value in the cases under scrutiny is 0.2 bar).

5. Results

The methane based expander bleed cycle configuration resulting from the present basic and parametric analyses is summarized in Fig. 8. Because of the benefits obtained in the nozzle extension cooling bypassing part of the fuel from

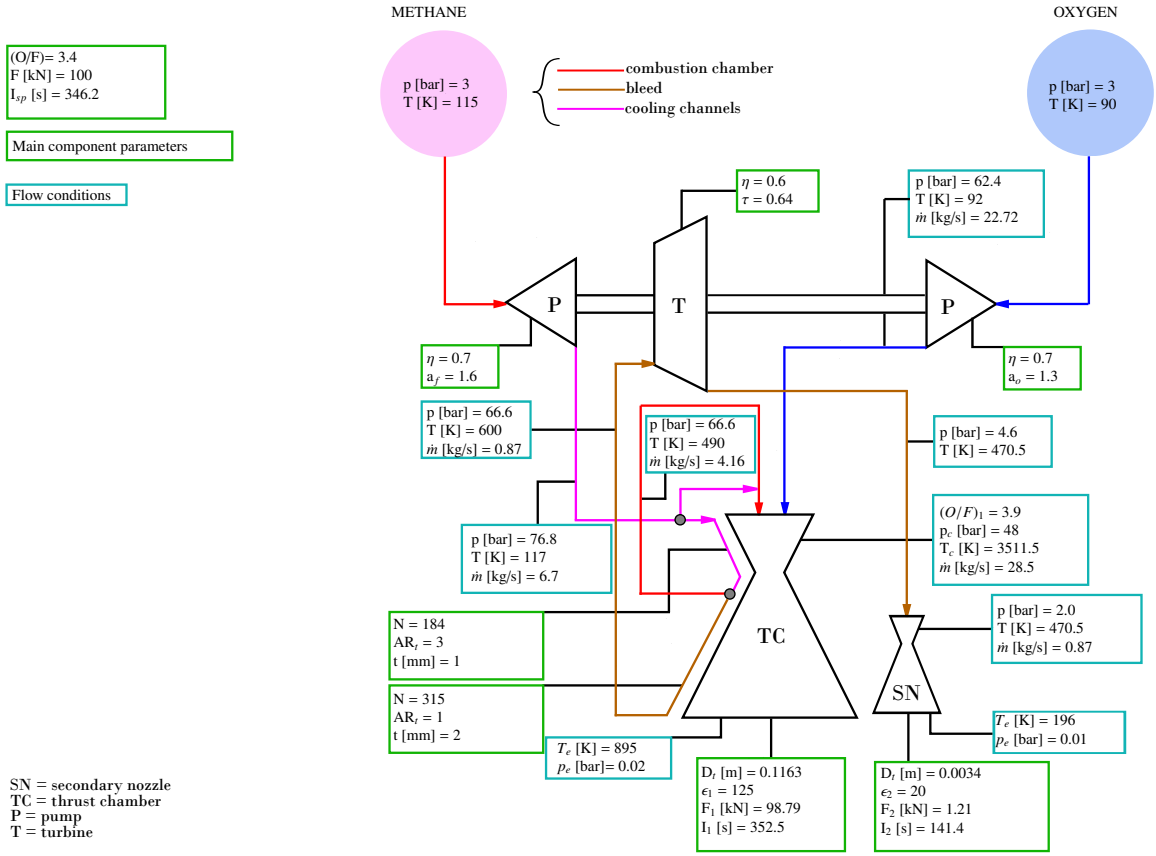

Figure 8: Flow schematic of the expander engine at reference design point

the main cooling system, this latter case has been considered ($\dot{m}_{f,cool} = 5.03$ kg/s), with aspect ratio of the main cooling system $AR_t = 3.0$. It is worth underlining that the present methane expander bleed system design has to be considered just as a possible starting point for an optimization process, where more precise constraints (in terms of material properties, turbomachine behavior, flow properties variation, pressure losses, ...) should be introduced. Nevertheless, this example shows as reasonable performance can be obtained by such a system, despite the conservative approach

DOI: 10.13009/EUCASS2017-332

followed. Further studies in the direction of optimizing the cycle and have a more detailed picture of the overall behavior of the cycle are necessary and are presently in progress.

6. Conclusion

A basic analysis on the feasibility of a methane-fueled expander bleed engine has been carried out. The results obtained for a configuration which fits with the foreseen environment for VEGA-E upper stage shows that the available methane flow rate is able to cool efficiently the engine and provide the power to drive turbines such to provide 48 bar chamber pressure. The amount of diverted mass flow rate is reasonable, being about 3% of the overall propellant mass flow rate. However, the secondary flow performance penalty is quite high, leading to 20 s lower specific impulse than the expected closed expander cycle engine performance. The evaluation of the cooling channel system has shown that the assumptions made in the basic analysis were excessively conservative, moreover a few seconds of specific impulse could be recovered if a higher turbine pressure ratio would be allowed. This detailed trade-off would require also the evaluation of the weight of all components and is therefore strongly related to the specific stage design and to the selection of engine materials.

References

[1] NIST, National Institute of Standards and Technology. http:// webbook.nist.gov/ chemistry/ fluid/ (retrieved June 09, 2017).

[2] P. Alliot, E. Dalbiès, and V. Delie. Overview of the development progress of the VINCI engine. In *54th International Astronautical Congress of the International Astronautical Federation, the International Academy of Astronautics, and the International Institute of Space Law*, Bremen, Germany, October 2003.

[3] D. R. Bartz. Turbulent boundary-layer heat transfer from rapidly accelerating flow of rocket combustion gases and of heated air. *Advances in Heat Transfer*, Vol. 2:pp. 2–108, 1965.

[4] C. Brown. Conceptual investigations for a methane-fueled expander rocket engine. AIAA Paper 2004-4210, 2004. 40th AIAA/ASME/SAE/ASEE Joint Propulsion Conference and Exhibit, Fort Lauderdale, Florida, doi: 10.2514/6.2004-4210.

[5] P. Caisso, A. Souchier, C. Rothmund, P. Alliot, C. Bonhomme, W. Zinner, R. Parsley, T. Neill, S. Forde, R. Starke, W. Wang, M. Takahashi, M. Atsumi, and D. Valentian. A liquid propulsion panorama. *Acta Astronautica*, 65(11-12):1723 – 1737, 2009.

[6] Empresarios Agrupados Internacional S.A. *EcosimPro 5.4. Modelling and Simulation Software*, 2015.

[7] Y. Fukushima and T. Imoto. Lessons learned in the development of the LE-5 and LE-7. In *30th AIAA/ASME/SAE/ASEE Joint Propulsion Conference*, Indianapolis, Indiana, June 1994. AIAA 94-3375.

[8] Y. Fukushima, H. Nakatsuzi, R. Nagao, K. Kishimoto, K. Hasegawa, T. Koganezawa, and S. Warashina. Development status of the LE-7A and LE-5B engines for H-IIA family. *Acta Astronautica*, 5(5):275–284, 2002.

[9] S. Gordon and B. J. McBride. Computer program for calculation of complex chemical equilibrium compositions and applications. Technical report, 1994. NASA Reference Publication 1311.

[10] A. Higashi, N. Nagao, H. Nanri, K. Okita, A. Ogawara, J. Takida, H. Sunakawa, K. Nakamura, T. Mizuno, S. Kono, and Y. Arimoto. Development of the 2nd stage engine for the next flagship launch vehicle “H3 launch vehicle”. In *Space Propulsion Conference*, Rome, Italy, 2016.

[11] Y. Kakuma, M. Yasui, O. Tadaoki, R. Sekita, and S. Warashina. LE-5B engine development. In *36th AIAA/ASME/SAE/ASEE Joint Propulsion Conference and Exhibit*, Huntsville, Alabama, July 2000. AIAA 2000-3775.

[12] H. Kawashima, S. Hori, T. Kobayashi, and K. Okita. Development of LE-9 engine. In *Space Propulsion Conference*, Rome, Italy, 2016.

[13] A. Kurosu, A. Ogawara, N. Yamanishi, T. Onga, A. Kumakawa, M. Nishimoto, H. Manako, and K. Okita. LE-X, Japan’s next generation booster engine. In *26th ISTS Conference*, Hamamatsu, Japan, June 2008. ISTS 2008-a-02.

DOI: 10.13009/EUCASS2017-332

[14] D. Manski, C. Goertz, H.-D. Saßnick, J. R. Hulka, B. D. Goracke, and D. J. H. Levack. Cycles for earth-to-orbit propulsion. *Journal of Propulsion and Power*, 14(5):588–604, 1998. doi: 10.2514/2.5351.

[15] H. Nagai, H. Taniguchi, I. Yamazaki, H. Maekawa, and T. Nakagawa. Development of H-II rocket second stage propulsion system. In *AIAA 25th Aerospace Sciences Meeting*, Reno, Nevada, January 1987. AIAA 87-0397.

[16] R. C. Parsley and B. Zhang. Thermodynamic power cycles for pump-fed liquid rocket engines. In V. Yang, M. Habiballah, M. Popp, and J. Hulka, editors, *Liquid Rocket Thrust Chambers : Aspects of Modeling, Analysis, and Design*, volume 200, Progress in Astronautics and Aeronautics Series, pages 621–648. AIAA, 2004.

[17] P. Pempie and L. Boccaletto. LOX/CH_4 expander upper stage engine. 55^{th} International Astronautical Congress, Oct. 2004.

[18] M. Rudnykh, S. Carapellese, D. Liuzzi, L. Arione, G. Caggiano, P. Bellomi, E. D'Aversa, R. Pellegrini, S. Lobov, A. Gurtovoy, and V. Rachuk. Development of lm10-mira lox/lng expander cycle demonstrator engine. *Acta Astronautica*, 126:364–374, 2016.

[19] J. Sannino, J. Delange, V. De Korver, A. Lekeux, and B. Vieille. Vinci propulsion system: Transition from Ariane 5 ME to Ariane 6. In *52nd AIAA/SAE/ASEE Joint Propulsion Conference*, Salt Lake City, UT 2016.

[20] J. R. Santiago. Evolution of the RL10 liquid rocket engine for a new upperstage propulsion. In *32nd AIAA/ASME/SAE/ASEE Joint Propulsion Conference and Exhibit*, Lake Buena Vista, Florida, July 1996. AIAA 96-3013.

[21] R. Sekita, M. Yasui, and S. Warashina. The LE-5 series development, approach to higher thrust, higher reliability and greater flexibility. In *36th AIAA/ASME/SAE/ASEE Joint Propulsion Conference and Exhibit*, Huntsville, Alabama, July 2000. AIAA 2000-3453.

[22] A. Urbano and F. Nasuti. Parametric analysis of cooling properties of candidate expander-cycle fuels. *Journal of Propulsion and Power*, 30(1):153–163, 2014.